Selective resonant ionization of zirconium isotopes using intermediate-state alignment

L.W. Green, G.A. McRae, and P.A. Rochefort
AECL Research, Chalk River, Ontario, Canada K0J 1J0
(Received 13 January 1993)

High selectivity (> 10) for separation of ^{91}Zr from other Zr isotopes was observed during triple resonant ionization of Zr vapors. Linearly polarized lasers were used to prepare aligned states, from which further excitation to a discovered $J = 0$ level could be suppressed for even-mass isotopes, by a suitable choice of relative laser polarization. Photoionization of the odd-mass isotope ^{91}Zr could be retained by use of transitions with relatively strong hyperfine interactions, because of associated population redistributions in the magnetic sublevels. The dependence of the even-mass-isotope signals on relative laser polarization followed sinusoidal forms, which are in excellent agreement with predictions derived from the geometric components of the transition dipole moment. The isotopic selectivity for ^{91}Zr can be increased by use of saturating fluences, because of the effects of saturation, population trapping in the even-mass isotopes, and strong hyperfine interactions in the odd-mass isotopes. For the same reasons, biases in even:odd isotope ratio measurements cannot always be eliminated by polarization scrambling or special angles.

PACS number(s): 32.30.−r, 32.80.Rm, 35.10.Bg, 35.10.Di

I. INTRODUCTION

Zirconium is a favored material for in-core components of nuclear power reactors because of its mechanical strength and the relatively low thermal neutron-capture cross sections of the various isotopes. The low cross sections are particularly important for CANDU (Canadian deuterium uranium) reactors, which require high neutron efficiency to permit the use of isotopically natural uranium dioxide fuels. Consequently, almost all in-core components of CANDU reactors are constructed from zirconium alloys, mostly Zr–2.5 wt % Nb, amounting to an inventory of 31 Mg per 600 MWe (megawatt electric) reactor. Reduction of the overall thermal neutron load would yield improved fuel economy or would allow the use of thicker, stronger fuel-channel components, which could give added safety and economic benefits.

Zirconium has five naturally occurring isotopes, one of which (mass 91) has a much higher cross section than the others. A tenfold depletion of the ^{91}Zr isotope to 1% would reduce the overall neutron-capture cross section from 0.25 to 0.1 b in the Zr–2.5 wt % Nb alloy. Further depletion of ^{91}Zr in this alloy would be of little value because of neutron absorption by Nb and ^{92}Zr.

Separation of ^{91}Zr is relatively difficult, because of its intermediate placement amongst the other isotopes and, because of its small optical isotope-shifts, e.g., 100–200 MHz [1–3]. An atomic vapor laser isotope separation (AVLIS) method has been proposed and is based on three-photon double-resonant ionization of Zr vapor [1,2]. In this scheme a pulsed single-longitudinal-mode dye laser is tuned to a group of hyperfine transitions which is slightly shifted from the even-mass isotope transitions. To improve selectivity, the Doppler line broadening, associated with vaporization temperatures of greater than 2200 °C, is suppressed by supersonic expansion of the vapor through a nozzle. A selectivity of greater than 10 is achieved [1] because of the relatively narrow bandwidth of the pulsed laser (500 MHz) and the cooling of the atoms during the expansion.

An alternative approach, based on intermediate-state alignment, is described in this paper. Linearly polarized, pulsed dye lasers are used to prepare aligned states from which further excitation of the even-mass isotopes is prohibited by selection rules. Hyperfine interactions in ^{91}Zr cause population redistributions which allow selective excitation and ionization of this isotope. High spectroscopic resolution is not necessary, permiting the use of broadband lasers and thermally distributed atomic vapors.

In similar work, circularly polarized light has been used to study intermediate-state evolution in Na [4]. A study of a two-photon interference effect for selective ionization of Ba and Sr isotopes [5], as well as a study of a multistep resonant ionization of Gd isotopes, in the presence of a magnetic field [6], has been reported. Alignment effects in uranium photoionization have been investigated in our laboratory [7,8].

II. THEORY

Three types of resonant transitions are of interest in this study. Type-(1) transitions are those for which J is a good quantum number. This description is expected to be suitable for the even-mass isotopes of Zr because they do not have nuclear spin ($I = 0$). The second, type (2), is similar to the first but includes the effects of hyperfine interactions which are weak compared to the resonant transition and slow compared to the pulse duration. The transition initially takes place as above; however, the excited state is perturbed by the weak hyperfine interaction and evolves in time. The third, type (3), is characterized by hyperfine interactions that are at least as important as the electric dipole interaction, and are fast compared to the pulse duration. For this type, F is the good quantum number.

A. Type (1)

A linearly polarized laser, tuned to an atomic resonance, induces an electronic transition from an initially isotropic ground state $|jm\rangle$ to an excited state $|JM\rangle$. The transition strength is nonuniformly distributed amongst the magnetic sublevels and the resulting population distribution in the excited state is anisotropic: the excited state is said to be aligned (i.e., sublevel populations vary as M^2 for $\Delta J = 0$ and as $J^2 - M^2$ and $j^2 - M^2$ for $\Delta J = +1$ and -1, respectively). In the current work, the alignment produced by a pulsed laser is probed, sometime later, by another laser for which the linearly polarized electric-field vector is rotated.

The lasers used in this study operate in multilongitudinal modes and are characterized by random fluctuations in frequency, intensity, and phase. These features, combined with the damping associated with Doppler broadening and decay, destroy the phase relationships in the transitions and yield incoherent behavior [9]. Consequently, for the transition $|jm\rangle \longrightarrow |JM\rangle$, the excited-state population distribution $P(J,M)$, in which M is quantized along the polarization axis of the subsequent laser pulse, is given by

$$P(J,M) \propto \sum_m |d^J_{Mm}(\theta)|^2 \begin{pmatrix} j & 1 & J \\ -m & 0 & M \end{pmatrix}^2 P(j,m), \quad (1)$$

where the initial population is $P(j,m)$. The $3j$ symbol describes the relative line strengths which lead to the alignment in the excited state, and the $d^J_{Mm}(\theta)$ are the reduced rotation matrix elements that transform this alignment onto the electric-field axis of the probe laser. Tables of $3j$ symbols and $d^J_{Mm}(\theta)$'s required for the calculations in this study can be found in [10]. The proportionality constant implicit in Eq. (1) includes the "dynamic" terms of the transition, which are separable (Wigner-Eckart theorem) from the geometric terms shown above.

The angular-momentum distribution can be expanded into multipole moments expressed in terms of spherical tensors: $A^{(k)}_q(J)$. The alignment includes all terms of even rank k. Characterization of the alignment, for any arbitrary angle between subsequent laser polarizations, requires the calculation of all the $|q| \leq k$ components. However, for relative laser polarizations of 0° and 90°, for which there is cylindrical symmetry, only the $q = 0$ component is nonzero. As an example, the quadrupole alignment is

$$A^{(2)}_0(J) = \frac{\sum_M P(J,M)\langle JM|3J_Z^2 - \mathbf{J}^2|JM\rangle}{\sum_M P(J,M)J(J+1)}. \quad (2)$$

This is the highest moment allowed for a $J = 1$ level. The alignment is positive if the population distribution favors large $|M|$, negative if small $|M|$ are favored, and zero if the relative polarizations are set to the magic angle of 54.7°, at which the distribution is isotopic.

The two extremes in alignment that can be prepared in the zirconium excitation sequence are illustrated in Fig. 1, for an example in which the relative angle of polarization θ_{12} between the first and second lasers is 90°. The relative sublevel populations, quantized along the polarization axis of the next laser pulse in the sequence, are obtained from Eq. (1) for each resonant step, with appropriate substitutions for initial levels. These aligned states are preserved during the time (nanoseconds) between photoexcitations, provided the atoms are not perturbed by collisions or by stray electric and magnetic fields. The ratio of the photoionization signal at these two extremes of the polarization of the probe laser, $i(\theta_{23} = 0°)/i(\theta_{23} = 90°)$, follows the alignment in the prepared state. This ratio is convenient to measure in the laboratory, and is readily predicted from Eq. (1).

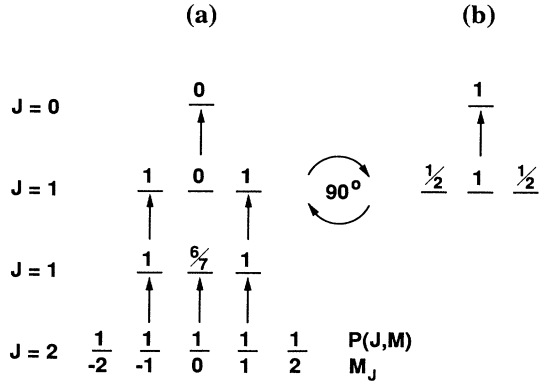

FIG. 1. Sublevel diagram showing relative populations $[P(J,M)]$ for a J = 2-1-1-0 excitation scheme (even-mass isotopes). $\theta_{12} = 90°$ and (a) $\theta_{23} = 0°$, (b) $\theta_{23} = 90°$. The strictly J-dependent contributions to the populations are not included. The populations are normalized to a maximum value of one in each sublevel.

B. Type (2)

^{91}Zr has nuclear spin $I = \frac{5}{2}$, and hyperfine splitting (hfs) constants (A) have been reported in the range of 5 to 300 MHz [3,11]. If the hfs is small compared to the Rabi frequency, then the transition proceeds as if J is a good quantum number. This produces spatially aligned intermediate states in the same way as expected for the even-mass isotopes. Following the pump pulse, the alignment is disrupted by the precession of J and I around F. The time evolution of the alignment is given by [10]

$$A^k_q(J;t) = G^{(k)}(t)A^k_q(J;0). \quad (3)$$

The function that propagates the alignment in time is

$$G^{(k)}(t) = \sum_{F,F'} \cos[(E_{F'} - E_F)t/\hbar] \frac{(2F'+1)(2F+1)}{2I+1} \times \begin{Bmatrix} F' & F & k \\ J & J & I \end{Bmatrix}^2, \quad (4)$$

where the term in curly brackets is a $6j$ symbol and

$E_F = (A/2\hbar)\,F(F+1)$ is the energy of the level F in the intermediate state. The alignment evolves periodically and its time average is reduced from its initial value.

C. Type (3)

For hyperfine splittings comparable to, or greater than, the Rabi frequency, the coupled $IJFM_F$ basis is used, and the alignment is invariant in time. Populations $P(F', M_F)$ are given by [9]

$$P(F', M_F) \propto \sum_F \begin{pmatrix} F & 1 & F' \\ -M_F & 0 & M_F \end{pmatrix}^2 (2F'+1)(2F+1) \times \begin{Bmatrix} J & 1 & J' \\ F' & I & F \end{Bmatrix}^2 P(F, M_F). \quad (5)$$

The alignment is reduced compared to that in J because of the larger number of levels and sublevels, and the new linkages between them [9]. The new linkages allow access to all sublevels.

D. Saturation effects

Atomic transitions are readily saturated, e.g., at fluences as low as 10 mJ/cm^2, by pulsed dye lasers tuned to resonant frequencies. For the incoherent transitions studied here, the rate-equation model is appropriate and saturation corresponds to near-equal populations in upper and lower levels. Furthermore, the population tends to be equalized across sublevels, as long as each individual sublevel transition is saturated. Sublevel transitions forbidden by selection rules are excepted, and, for these, the population remains trapped in the lower sublevel until lost by spontaneous decay.

E. Selective ionization

An important result of alignment and hyperfine interactions is that selective ionization of ^{91}Zr should be possible, with a suitable choice of angular-momentum quantum numbers, polarization, laser fluence, and delay between laser pulses. This is because the conditions, which block photoionization pathways in the even-mass isotopes, are changed in the odd-mass isotope by hyperfine-induced population redistribution. The objectives of this work are to identify zirconium excitation sequences and characterize them according to their geometric and dynamic properties so that conditions yielding the highest isotopic selectivity can be identified.

III. EXPERIMENT

Zirconium atomic vapors were generated thermally by resistive heating of a rhenium filament onto which 0.7 mg of Zr metal was spot welded. The filament was mounted in the ion source of a 5-m time-of-flight mass spectrometer, as described previously [12]. The resolution $(m/\Delta m)$ of the mass spectrometer for Zr was typically 500 (Fig. 2). Filament temperatures of 1800 °C were used and ion-source electrode voltages were adjusted to reduce thermal ionization signals to negligible levels.

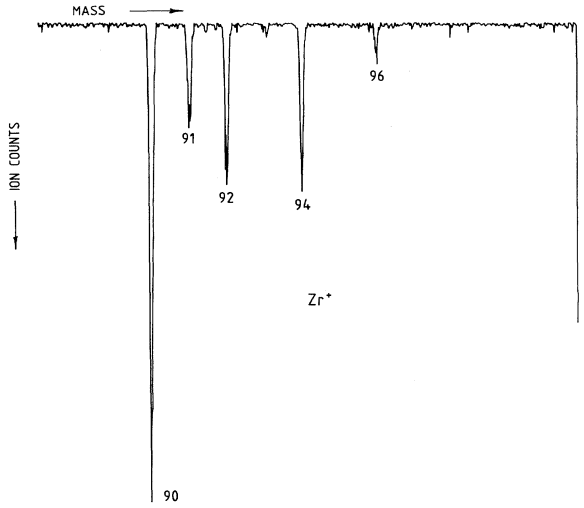

FIG. 2. Time-of-flight mass spectrum of Zr averaged over 10^6 laser pulses.

Two Lumonics (Model Hyperdye 300) tunable dye lasers pumped by an Oxford (Model CU40) copper vapor laser (CVL) were used for resonant excitation (Fig. 3). The CVL was operated at 5.0 kHz with unstable resonator optics, and, after beam telescoping and splitting, delivered a power of ~10 W of green light (510 nm) to the oscillator cell of each dye laser. A home-built, 3-W, resistively heated CVL was used to pump a third dye laser. Two of the dye lasers were charged with rhodamine 590 (R590) dye, and the other with rhodamine 575. The dye lasers delivered pulse energies of ~4 μJ over bandwidths of ~0.05 cm^{-1} (full width at half maxima). The radial profiles of the dye-laser beams were roughly Gaussian with $1/e^2$ beam radii of $r_0 = 0.1$ mm. Amplifier cells and associated optics were not used. Pulses were ~ 13 ns in duration with some spiking. A Stanford Research Systems Delay Generator (DG 535) was used to control and synchronize the CVL's. Dye pulses were delayed with respect to each other either electronically or optically; for the electronically delayed pulses the "jitter" was ±3 ns. The yellow output, 578 nm, of one of the CVL's was used for ionization from the high level states. The laser energy was varied with colored filters and a Molectron joulemeter (J3-09 modified for 10 kHz) was used to measure pulse energies.

The dye circulation system was designed to provide a high flow rate, 7 l/min, with minimal vibrations. A 3.7-l stainless-steel reservoir was placed in the flow line on both sides of a Micropump (Model 81379) pump. All flow lines were made from 1.2-cm-i.d. Teflon tubing and the dye cell walls were bored out to allow unrestricted flow of the dye. The resultant dye flow was very smooth and bubble-free, as well as being fast enough for CVL pumping. The dye was water cooled to avoid degradation. With careful alignment of the lasers, bandwidths of 0.04 cm^{-1} could be obtained with excellent line stability. Frequency analysis showed that there was structure within the bandwidth due to the multimode nature of the

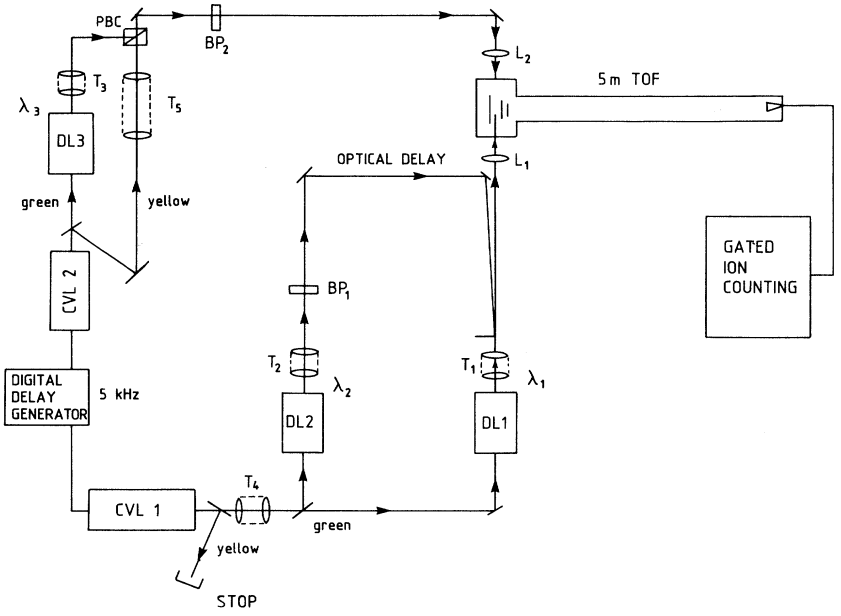

FIG. 3. Schematic of apparatus: CVL, copper vapor laser; DL, dye laser; T, telescope; L, lens; PBC, prism beam combiner; BP, birefingent $\lambda/2$ plate; TOF, time-of-flight mass spectrometer.

oscillator. The laser beams were linearly polarized, and the plane of polarization was rotated using a $\lambda/2$ birefringent plate. The $\lambda/2$ plate was carefully positioned to avoid beam "walk-off," which was checked by observing a projection of the beam on a distant target during rotation of the plate.

Laser-induced-fluorescence (LIF) spectra of I_2 were recorded for wavelength calibration [12]. The LIF signals were generated by directing 5% of the laser beam to a cell which contained 0.2 Torr of I_2 and which was equipped with a Hamamatsu R106 photomultiplier detector. Iodine LIF and Zr resonance ionization spectra were monitored with a Stanford Research Systems SR250 boxcar averager, and stored for future spectral calibrations [12].

Photoionization signals were recorded in the ion-counting mode, using a fast Galileo Model FTD 2003 microchannel plate detector. A multichannel gated pulse-counting system [13,14] was used for simultaneous counting of many isotopes. Four channels were used in this work, one each for mass 90, 91, and 92, and one for background measurement. Gate widths were set to 200 ns, and count durations were set to 10^6 CVL pulses to obtain sufficient counting precision. The background was monitored near mass 88. The count totals ranged between 100 and 5000 per isotope.

IV. RESULTS AND DISCUSSION

A. Excitation schemes

Zirconium is characterized by an a^3F_2 ground state and an ionization potential of 53 506.0 cm^{-1} above this level [1]. Double-resonant excitation, via known $J = 1$ states [15], steps I and II of Fig. 4, was chosen to prepare intermediate-state alignments as depicted in Fig. 1. Ten previously unobserved high-lying states (Table I) were discovered by scanning a third laser over the range of R590 dye, and their energies were determined by comparison with I_2 LIF. The J assignments for three of these (Table I) were determined by rotation of the relative polarizations of the lasers for λ_2 and λ_3, as discussed later. Excitation schemes I-II-IV and I-II-V (Fig. 4) were chosen for polarization studies because of their potential for showing large alignment effects. As work progressed, the I-III-VI scheme was included.

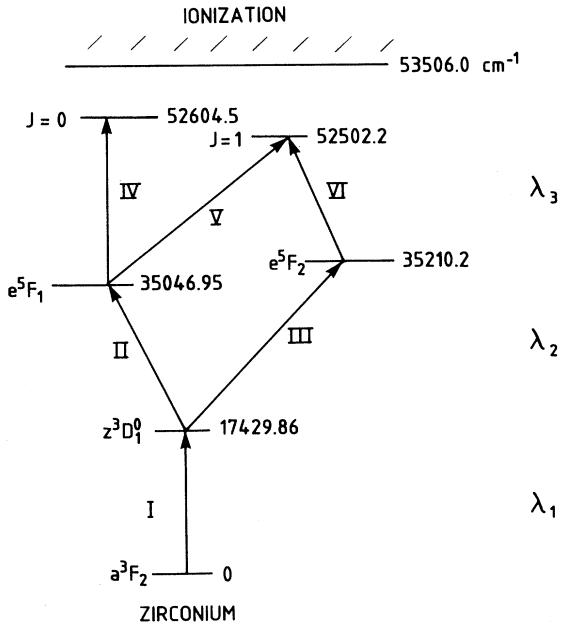

FIG. 4. Excitation pathways used in this work. The yellow 578-nm beam of the CVL was used for ionization. I, 573.8 nm; II, 567.6 nm; III, 562.4 nm; IV, 569.6 nm; V, 572.9 nm; VI, 578.3 nm.

TABLE I. Observed high-lying states in zirconium.

E (cm^{-1})	J
51939.1	
52057.8	
52076.1	
52161.0	
52167.97	
52174.14	1
52278.04	
52287.5	
52502.2	1
52604.47	0

B. Transition parameters

Excited-state lifetimes were determined by recording the decrease of the photoionization signal as the delay between the pump and the probe sequences was increased electronically. Depending on which lifetime was being measured, the pump sequence contained one (or two) of the different color laser pulses, and the probe sequence contained three (or two) different color pulses. All laser pulses within each sequence were maintained at a constant optical delay of 20 ns with respect to each other. Results were fitted to

$$i/i_0 = \exp(-t/\tau), \tag{6}$$

where τ is the lifetime and i and i_0 are the photoionization signals at pump-probe delay times t and $t = 0$, respectively. Each datum, in these and later fits, was weighted by the squared inverse of the experimental error. The error in ion counts was taken as the square root of the number of counts. Branching ratios were not determined. An example of excited-state decay is shown in Fig. 5 for the 35 210.2-cm^{-1} state. Good agreement is observed between decay data for ^{90}Zr, ^{91}Zr, and ^{92}Zr. Similar agreement was found for the decay measurement of the 35 046.95-cm^{-1} state. This similarity between even- and odd-mass isotope decay demonstrates that there is no time evolution of the alignment in the odd-mass isotope within the delay times studied. Lifetimes can be measured without the complication of the time evolution of the alignment, if necessary, by setting the relative laser polarizations at the magic angle.

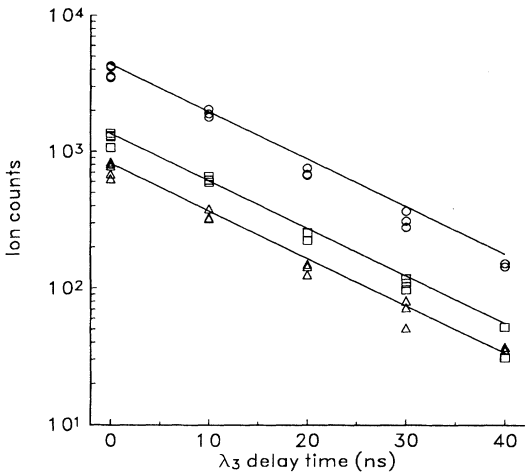

FIG. 5. Spontaneous decay of the 35 210.2-cm^{-1} state with step VI as a probe and $\theta_{23} = 0°$. The observed lifetime is 13±5 ns. Similarly, the lifetime for the 35 046.95-cm^{-1} state is 11±2 ns. The fits include a linear-loss term to account for sample consumption; however, the lines shown above are drawn from only the exponential term [Eq. (6)]: ○, ^{90}Zr; □, ^{91}Zr; △, ^{92}Zr.

The lifetime measurements were frequently influenced by sample consumption. This was corrected for by including a linear-loss term which multiplies the exponential in Eq. (6). The resultant lifetimes of the states at 35 046.95 and 35 210.2 cm^{-1} are 11±2 and 13±5 ns, respectively. In these experiments there was no indication of any effects due to the drift of atoms away from the filament and out of the illuminated detection volume. However, in the lifetime measurement for the longer-lived 17 429.86-cm^{-1} state, shifts in ion flight times were observed. This is attributed to atomic drift and, accordingly, the lifetime of this state is reported as a lower limit ($\geq$ 230 ns).

Photon-absorption cross sections (σ) were estimated from the fluence dependence of the photoionization signal. Each transition was treated as an independent two-level system, since the laser pulses were separated in time. The ion signal is expected to follow an exponential dependence on the photon fluence $\Phi(r)$ [9]

$$i(\Phi(r)) = \eta\{1 - \exp[-\sigma\Phi(r)/\hbar\omega]\}, \tag{7}$$

where η is an efficiency factor. Integration of Eq. (7) over the volume illuminated by the Gaussian laser beam yields

$$i_G(\Phi_0) = \eta' [E_1(\sigma_{\text{eff}}E) + \gamma + \ln(\sigma_{\text{eff}}E)], \tag{8}$$

where E_1 is the exponential integral, $\gamma = 0.577\,21\ldots$ is Euler's constant, E is the radiant energy per pulse, $\sigma = \frac{1}{2}\pi r_0^2 \hbar\omega\sigma_{\text{eff}}$, and r_0 is the $1/e^2$ radius. The σ_{eff} and η' were obtained by fitting the ionization signals as a function of the energy per pulse to Eq. (8).

An example of photoionization yield versus laser energy is shown in Fig. 6 for step III. The linear dependence of the ion yield on the logarithm of the laser energy indicates that, at the center of the beam, transition III was saturated over the range of energies used. Similar results were obtained for transitions II and VI. Signal increase is attributed to increased ionization from the unsaturated wings of the laser beam as the fluence is increased. Although the effective cross sections are reasonably well known, the absolute cross sections cannot be reported with precision. This is because of the uncertainties in the effective beam radius due to difficulties in obtaining reproducible overlap of the four beams. These difficulties are reflected in the poor quality of the fit for the data in Fig. 6; the value of χ^2 is 25 for 7 degrees of freedom. Assuming the lasers are Gaussian with beam radii of 0.1 mm, cross-section order-of-magnitude estimates are 10^{-15} cm^2 for transitions II and III, and 10^{-16} cm^2 for transition VI. For transition I, the ionization sig-

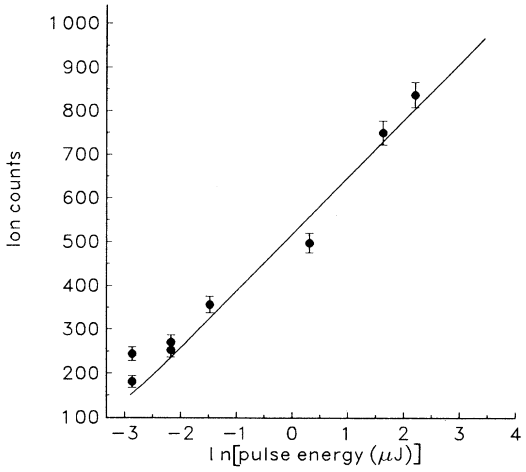

FIG. 6. Dependence of the ionization signal on pulse energy of λ_2 in transition III. The linear dependence of the ion signal on the logarithm of the pulse energy indicates saturation of the transition.

nal depended linearly on the pulse energy with no signs of saturation, over the pulse energies used in this study. Consequently, for transition I, the parameters η' and σ_{eff} could not be separated.

C. Alignment

In this series of experiments θ_{23} is varied, and the ionization signal is expected to be proportional to the sum of the populations $P(J,M)$ excited by λ_3. This sum is dependent on the population distribution prepared by λ_2 and on the M-dependent line strengths of the subsequent transition. For the even-mass isotopes of scheme I-II-IV (Fig. 1), the population excited by λ_3 is [Eq. (1)]

$$P(0,0) \propto \tfrac{7}{2}\sin^2\theta_{23} \tag{9}$$

and for scheme I-II-V, $P(1,0) = 0$ and

$$P(1,\pm1) \propto \tfrac{7}{4}(1+\cos^2\theta_{23}). \tag{10}$$

These are type-(1) transitions, in which the angle θ_{12} between the first two laser polarizations is set to 90°. The implicit proportionality constant contains the strictly J-dependent terms that cancel when signal ratios are considered. The ionization step was found to be independent of the polarization angle θ_{34}.

The ^{91}Zr signal showed no dependence on relative polarization and, furthermore, its $i(\theta_{23}=0°)/i(\theta_{23}=90°)$ $(= 1.1 \pm 0.1)$ ratio was independent of delay time. It therefore provided a convenient internal reference. Results for the 90:91 and 92:91 Zr ratios of scheme I-II-IV and I-II-V, measured as a function of θ_{23}, show evidence of the strong alignment expected in the 35 046.95 cm^{-1} state of the even-mass isotopes (Figs. 7 and 8). This alignment persists at higher fluences, even beyond saturation, because step II involves only three sublevel transitions, one of which is forbidden. The lack of polarization dependence in ^{91}Zr indicates that the populations in the magnetic sublevels are equalized by hyperfine interactions and saturation effects. If the initial state for each transition in the odd isotope is assumed to be isotropic, then the even:odd isotope ionization ratio is expected to vary as

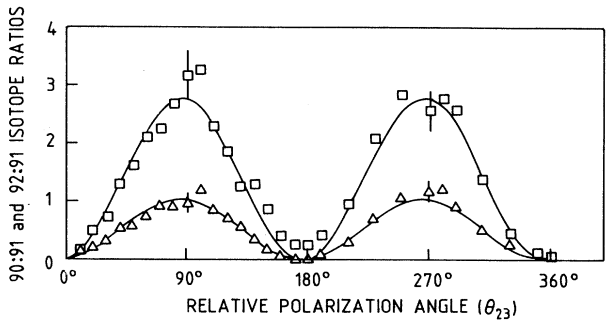

FIG. 7. Dependence of even:odd isotopic ratio on θ_{23} for the I-II-IV (J = 2-1-1-0) scheme. □, 90:91; △, 92:91. The curves are drawn from the best-fit equations: 90:91 ratio = $2.78(9)\sin^2[\theta_{23} + 3(1)]$ and 92:91 ratio = $1.03(4)\sin^2[\theta_{23} + 5(2)]$ (the numbers in parentheses are the standard deviations in units of least significant figure). A delay time of 20 ns between laser pulses was used for the data here and in Fig. 8.

$$\frac{(\text{even}:\text{odd})}{(\text{even}:\text{odd})_{\text{natural}}} = \tfrac{63}{40}\sin^2\theta_{23} \tag{11}$$

for J(final)= 0 (I-II-IV), and

$$\frac{(\text{even}:\text{odd})}{(\text{even}:\text{odd})_{\text{natural}}} = \tfrac{63}{80}(1+\cos^2\theta_{23}) \tag{12}$$

for J(final)= 1 (I-II-V). The smooth curves drawn in Figs. 7 and 8 are calculated from best fits to the functional forms of Eqs. (11) and (12), where the effective

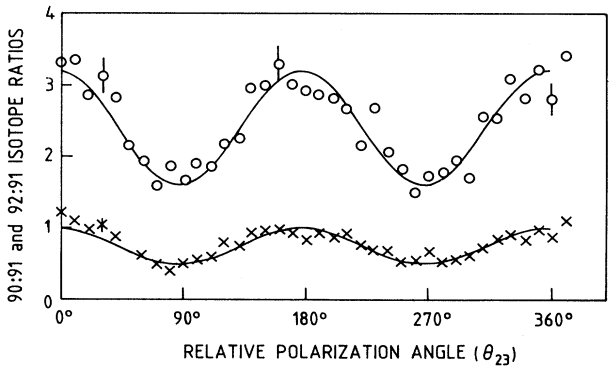

FIG. 8. Dependence of even:odd isotopic ratio on θ_{23} for the I-II-V (J = 2-1-1-1) scheme. ○, 90:91; ×, 92:91. The curves are drawn from the best-fit equations: 90:91 ratio = $1.60(2)\{1 + \cos^2[\theta_{23} + 3(2)]\}$ and 92:91 ratio = $0.498(7)\{1 + \cos^2[\theta_{23} + 3(2)]\}$ (see Fig. 7 for additional comments).

coefficient and the definition of zero angle are varied.

The matrix elements responsible for these transitions factor into the product of two terms, one of which expresses the geometry, symmetry, and selection rules of the system, and the other which contains the dynamics (Wigner-Eckart theorem). The fits to the angular-dependent functional forms [Eqs. (11) and (12)] are as follows: 90:91 $= 2.78(9)\sin^2[\theta_{23} + 3(1)]$ and 92:91 $= 1.03(4)\sin^2[\theta_{23} + 5(2)]$, for scheme I-II-IV, and 90:91 $= 1.60(2)\{1+\cos^2[\theta_{23}+3(2)]\}$ and 92:91 $= 0.498(7)\{1+\cos^2[\theta_{23}+3(2)]\}$, for scheme I-II-V, where the numbers in parentheses are standard deviations in units of the least significant figure. The good quality of the fits show that the angular-momentum distribution in the excited Zr vapors is exactly as predicted. The observed isotopic ratios, after correction for the 90:91 and 92:91 natural abundance ratios of 4.6 and 1.5, respectively, are lower than the values predicted from the geometric arguments. This is explained by the saturation effects described in Sec. IV D.

For temporally separated laser pulses, suppression of the even-mass isotope signals is almost complete at parallel laser polarizations with J(final)=0 (Fig. 7), and the isotope selectivity [(90:91)prod./(90:91)feed] is greater than 10. Excitation to the $J = 0$ state is prohibited because of the lack of population in the $M = 0$ sublevel in the upper $J = 1$ state [Fig. 1(a)]. If $\theta_{23} = 90°$, the sublevel populations in the reference frame of the third (probe) laser are as described in Fig. 1(b), and photoionization is possible. The condition $\theta_{23} = 0$ yields the maximum isotopic selectivity for a laser-based isotope separation scheme.

Strong alignment was also observed in the I-III-VI scheme (Fig. 9). For the even-mass isotopes, the photoionization signal is predicted to have the following θ_{23} dependence:

$$i(\theta_{23}) \propto 43 + 75\cos^2\theta_{23}, \tag{13}$$

where in Eq. (1) θ_{12} has been set at the experimental value of 0°. The ratio $i(\theta_{23} = 0°)/i(\theta_{23} = 90°)$ (Fig. 9) is observed to be 2.8 ±0.3 for $\Delta t_{23} > 10$ ns (temporally resolved pulses) for ^{90}Zr; this value is in agreement with the expected value of 2.74 [Eq. (13)]. For delay times for which there is temporal overlap of the second and third laser pulses, $\Delta t_{23} < 10$ ns, the $i(\theta_{23} = 0°)/i(\theta_{23} = 90°)$ ratio decreases to 2.1±0.1 for ^{90}Zr. The reason for this decrease is not known; however, temporal overlap of nonparallel laser fields possibly allows the $M = \pm 2$ sublevels in the upper $J = 2$ level (35 210.2 cm^{-1}) to be accessed by $\Delta M = \pm 1$ transitions.

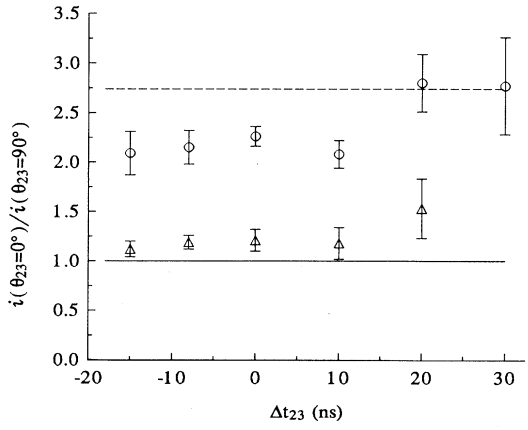

FIG. 9. Ratio of the photoionization signals for scheme I-III-VI at $\theta_{23} = 0°$ and 90° vs the delay time Δt_{23} between λ_2 and λ_3: ○, ^{90}Zr; △, ^{91}Zr. The dashed line shows the predicted value of 2.74 for the even-mass isotope, which is observed only when the pulses are separated in time.

For the odd-mass isotope in the I-III-VI scheme, the $i(\theta_{23} = 0°)/i(\theta_{23} = 90°)$ ratio is 1.18 ± 0.05, at delay times $\Delta t_{23} < 10$ ns. This evidence of a small alignment indicates that the hyperfine interaction in transition III is of intermediate strength [type (2)]. A lack of hyperfine interaction in step III [type (1)] would result in behavior similar to that seen for the even-mass isotopes. Strong hyperfine interactions [type (3)] would cause the $i(\theta_{23} = 0°)/i(\theta_{23} = 90°)$ ratio to equal 1.0 at all angles, because step III is saturated (Fig. 6). Strong hyperfine interactions in step VI would likewise nullify the effects of alignment introduced by step III, because step VI is also saturated (Sec. IV B). Therefore, step VI in ^{91}Zr must be a type-(2) transition with relatively weak hyperfine interactions. When the pulses are temporally resolved, $\Delta t_{23} > 10$ ns, the $i(\theta_{23} = 0°)/i(\theta_{23} = 90°)$ ratio for ^{91}Zr increases by the same proportion as the even-mass isotopes (Fig. 9).

Several tests were conducted to ensure that the data in Figs. 7, 8, and 9 were not affected by beam "walk-off" nor by static fields in the ion source. These included changing the initial axis of reference, changing which laser polarization was rotated, and rotating both laser polarizations in the same, and opposite, directions. The results showed that polarization effects were entirely due to the relative polarization of the two lasers, and hence confirmed the lack of influence of source fields and beam walk-off on the data.

D. Isotope ratios

The geometric arguments described above do not completely account for the observed even:odd results. The isotopic ratios (Figs. 7 and 8) measured for schemes I-II-IV and -V are lower than both natural abundance and, the values predicted with Eq. (1) (Table II), assuming a uniform population distribution for ^{91}Zr. However, the isotopic ratios measured for the nonresonant ZrO^+ signal and the one-color (scheme I) Zr^+ signal are in good agreement with expected (natural) values (Table II). This indicates that the low ratios reported above are because of transition phenomena in steps II and above rather than biases in the ion-counting system.

No alignment was observed in ^{91}Zr in the I-II schemes, even in experiments in which λ_3 was delivered as soon as possible after λ_2. This suggests that the hyperfine interaction is very fast, with a period of less than 20 ns, and that step II in the odd-mass isotope is a type-(3) transition. Accordingly, there are many linkages between

TABLE II. ^{90}Zr:^{91}Zr ratios for various excitation schemes. No alignment in ^{91}Zr is assumed in the predictions, except for the range 8.1 $\leftrightarrow$ 4.6 in scheme I-III-VI. $\theta_{12} = 90°$ and 0° for the series that involve I-II and I-III, respectively. Saturation refers to steps II, III, and VI only. Step I is not saturated, and the degree of saturation of steps IV and V is not known.

Scheme	θ_{23}	^{90}Zr:^{91}Zr ratio		
		Geometric prediction		Observed
		No saturation	Saturation	
Nonresonant ZrO^+		4.6	4.6	4.5 ±0.1
I		4.6	4.6	4 ±1
I-II-IV	90°	7.25	3.21	2.8 ±0.1
I-II-V	0°	7.25	3.21	3.20 ±0.04
I-III-VI	0°	8.1	8.1 $\leftrightarrow$ 4.6	5.2 ±0.4

sublevels [9], and all sublevels are equally excited, if the transition is saturated. This is not true for the lower $J = 1$ level in the even isotope, and $\frac{3}{10}$ of the population of this level are trapped in the $M = 0$ state. For the I-II schemes, the net result is that the even:odd isotope ratio is expected to be 30% lower, at saturation conditions for step II. In the absence of population trapping, the 90:91 and 92:91 ratios are expected to be the natural abundance values 4.6 and 1.5, respectively, at $\theta_{23} = 90°$ for scheme I-II-IV and 0° for I-II-V. Because of population trapping these predictions are lowered to 3.21 and 1.05, which are in good agreement with the observed results (Table II, Figs. 7 and 8). Not shown in the table are the experimental results for (92:91): 1.03 ±0.04 (I-II-IV) and 1.00 ±0.01 (I-II-V).

The influence of saturation and hyperfine interactions on the λ_3 transitions needs to be considered. For example, in scheme I-II-V, if hyperfine interactions are weak in both of the levels of the third step, transformation of the $IJFM_F$ population distribution prepared in the 35 046.95-cm^{-1} state to the JM basis is appropriate. The resultant distribution is isotropic, even at fluences below saturation, which is consistent with the observation of no alignment in ^{91}Zr. If hyperfine interactions are strong in the third transition, Eq. (5) must be reapplied. The result, at fluences below saturation, is a slight anisotropy, leading to, for example in scheme I-II-V, a 15% reduction in the photoionization rate for $\theta_{23} = 90°$ compared to 0°. This difference would be suppressed by saturation of step V. In scheme I-II-IV, the combination of saturation and strong hyperfine interactions in step IV would result in twice as much excitation out of the 35 046.95-cm^{-1} state of the odd-mass isotope compared to the even. The observed isotope ratios (Fig. 7 and Table II) indicate that these conditions were not met for step IV.

The isotopic ratios observed for scheme I-III-VI also differ from the natural values (Table II). In contrast to the I-II schemes, there are no inaccessible sublevels which can be populated in the even-mass isotopes at $\theta_{23} = 0°$. Therefore, the observed 90:91 ratio of 5.2 (Table II) indicates that not all of the population in the odd-mass isotope is accessed. This can be explained by population trapping. Step III is a type-(2) transition (Sec. IV C) and some population evolves [Eq. (3)] into the $M = \pm 2$ sublevels of the 35 210.2-cm^{-1} level in ^{91}Zr. This $M = \pm 2$ population is not fully accessed by the next transition because step VI, although saturated (Sec. IV B), is a type-(2) transition with a relatively weak hyperfine interaction (Sec. IV C). The result is a lower relative photoionization rate for the odd-mass isotope and a higher even:odd ratio. If step VI is a type-(3) transition, all sublevels would be equally accessible at saturation, and the observed isotope ratio would be natural.

These results show that the even:odd isotope ratios measured using resonance ionization techniques can be significantly different from the true values, and that the deviation can be either positive or negative. The combined effects of saturation, hyperfine interactions, and population trapping cause the even-mass isotopes to be favored in scheme I-III-VI, whereas in the I-II schemes, the same phenomena cause the odd-mass isotope to be favored. These biases cannot be avoided by setting the laser polarizations at the "magic angle" of 54.7°, although all sublevels are equally populated [Eq. (1)]. Furthermore, commonly used techniques such as polarization scrambling will not overcome the problems associated with the combination of inaccessible levels, saturation, and hyperfine coupling.

V. CONCLUSIONS

Selective resonant ionization of zirconium isotopes is possible by use of intermediate-state alignment and dynamics. Scheme I-II-IV is well suited for resonant depletion of ^{91}Zr, yielding a selectivity of greater than 10 when the polarizations of steps II and IV are parallel. This scheme takes advantage of the suppression of even-mass-isotope ionization by selection rules and selective alignment, and of the hyperfine-induced population redistribution in ^{91}Zr. The selectivity is achieved without use of high-resolution lasers or Doppler-cooled atomic beams and is enhanced by saturation effects. The selectivity is sufficient to allow improved fuel economy and/or stronger components in nuclear reactors.

The experimentally determined dependence of the ionization signal on the relative laser polarizations is in agreement with the dependence predicted from sublevel line strengths and reduced rotation matrix elements. This angular dependence can be applied to the assignment of angular-momentum quantum numbers. For example, if $\Delta J(\lambda_3) = \pm 1$, the signal increases as θ_{23} is changed from 0° to 90° (Fig. 7). Likewise, if $\Delta J = 0$,

the signal decreases as θ_{23} is changed from 0° to 90° (Fig. 8). Using this technique, if J of the initial state is known, then J of the final state can be deduced.

This study shows that saturation of transitions with strong hyperfine coupling leads to even:odd isotope ratios which are significantly different than natural. The strong dependence of the even:odd isotopic ratios on hyperfine coupling strengths, laser intensities (saturation), polarizations, and time delay between pulses, demonstrates that care must be taken when using resonant excitations in analytical applications (e.g., resonance ionization mass spectroscopy). For example, the required accuracy of isotope ratios is typically better than ~1%, yet biases of 200% and 300% are possible and, in the I-II-IV scheme, the even:odd ratio can be made zero with a suitable choice of laser polarization. Such unequal photoionizations of even- and odd-mass isotopes cannot always be avoided by commonly used techniques such as polarization scrambling or magic angle.

ACKNOWLEDGMENTS

The authors would like to acknowledge the technical support of F.C. Sopchyshyn, E.B. Selkirk, and H.M. Adams. Helpful discussions with G.A. Bickel are appreciated.

[1] P.A. Hackett, H.D. Morrison, O.L. Bourne, B. Simard, and D.M. Rayner, J. Opt. Soc. Am. B **5**, 2409 (1988).
[2] M.R. Humphries, O.L. Bourne, and P.A. Hackett, Chem. Phys. Lett. **118**, 134 (1985).
[3] W. Berres, D. Rusbult, E. Hintz, and H.L. Bay, Appl. Phys. B **35**, 83 (1984).
[4] T.W. Ducas, M.G. Littman, and M.L. Zimmerman, Phys. Rev. Lett. **35**, 1752 (1975).
[5] S.M. Park and G.J. Diebold, Phys. Rev. A **42**, 417 (1990).
[6] E. Le Guyadec, J. Ravoire, R. Botter, F. Lambert, and A. Petit, Opt. Commun. **76**, 34 (1990).
[7] L.W. Green, M.H.C. Smyth, P.A. Rochefort, and G.A. McRae, in *Polarization and Isotope Shift Effects in Uranium Isotope Ratio Measurements by Resonance Ionization Mass Spectrometry*, Proceedings of the 5th International Symposium on Resonance Ionization Spectroscopy and its Applications, edited by J.E. Parks and N. Omenetto, IOP Conf. Proc. No. 114 (Institute of Physics and Physical Society, Bristol, 1991), p. 243.
[8] L.W. Green, G.A. McRae and J.H. Rowat, in *Alignment and Dynamics During Resonant Excitation* (Ref. [7]), p. 113.
[9] B.W. Shore, *The Theory of Coherent Atomic Excitation* (Wiley, New York, 1990), Vols. 1 and 2.
[10] R.N. Zare, *Angular Momentum* (Wiley, New York, 1988).
[11] S. Buttgenbach, R. Dicke, H. Gebauer, R. Kuhnen, and F. Traber, Z. Phys. A **286**, 125 (1978).
[12] M.H.C. Smyth, L.W. Green, F.C. Sopchyshyn, and P.K. Leeson, J. Phys. B **24**, 4887 (1991).
[13] L.W. Green and F.C. Sopchyshyn, Int. J. Mass Spectrom. Ion Proc. **89**, 81 (1989).
[14] L.W. Green, R.G. Macdonald, and F.C. Sopchyshyn, Anal. Instrum. **17**, 195 (1988).
[15] C.E. Moore, *Atomic Energy Levels*, Natl. Bur. Stand. (U.S.) Circ. No. 467 (U.S. GPO, Washington, D.C., 1949).